2021 43rd Annual International Conference of the
IEEE Engineering in Medicine & Biology Society (EMBC)
Oct 31 - Nov 4, 2021. Virtual Conference

# Feasibility of Brain Imaging Using a Digital Surround Technology Body Coil: A Study Based on SRGAN-VGG Convolutional Neural Networks *

Ya-Wen Liu, Hai-Jun Niu, Hong-Xia Yin, Jing-Jing Xia, Peng-Ling Ren, Ting-Ting Zhang, Jing Li, Han Lv, He-Yu Ding, Jian-Liang Ren, Zhen-Chang Wang

***Abstract* — Brain imaging using conventional head coils presents several problems in routine magnetic resonance (MR) examination, such as anxiety and claustrophobic reactions during scanning with a head coil, photon attenuation caused by the MRI head coil in positron emission tomography (PET)/MRI, and coil constraints in intraoperative MRI or MRI-guided radiotherapy. In this paper, we propose a super resolution generative adversarial (SRGAN-VGG) network-based approach to enhance low-quality brain images scanned with body coils. Two types of T1 fluid-attenuated inversion recovery (FLAIR) images scanned with different coils were obtained in this study: joint images of the head-neck coil and digital surround technology body coil (H+B images) and body coil images (B images). The deep learning (DL) model was trained using images acquired from 36 subjects and tested in 4 subjects. Both quantitative and qualitative image quality assessment methods were performed during evaluation. Wilcoxon signed-rank tests were used for statistical analysis. Quantitative image quality assessment showed an improved structural similarity index (SSIM) and peak signal-to-noise ratio (PSNR) in gray matter and cerebrospinal fluid (CSF) tissues for DL images compared with B images ($P < .01$), while the mean square error (MSE) was significantly decreased ($P < .05$). The analysis also showed that the natural image quality evaluator (NIQE) and blind image quality index (BIQI) were significantly lower for DL images than for B images ($P < .0001$). Qualitative scoring results indicated that DL images showed an improved SNR, image contrast and sharpness ($P < .0001$). The outcomes of this study preliminarily indicate that body coils can be used in brain imaging, making it possible to expand the application of MR-based brain imaging.**

## I. Introduction

Magnetic resonance imaging (MRI) has been widely used as an in vivo imaging technique due to its safe, nonintrusive nature and high resolution. In particular, MRI has many applications in brain imaging because it is useful in an environment with many hydrogen nuclei and little contrast density [1]. In general, the scanning procedure for brain imaging requires patients to first have their head inserted with a head coil into the scanner and remain in that position for a long time [2]. However, conventional head coils present the following problems in practical applications. (a) Photon attenuation due to MRI head coils in positron emission tomography (PET)/MRI. In PET/magnetic resonance (MR) systems, MR head coils may be a potential source of image distortions and may degrade PET image quality due to additional attenuation and scatter [3-5]. (b) Coil constraints in intraoperative MRI or MRI-guided radiotherapy. The radiofrequency coils in intraoperative MRI systems need to be compatible with intraoperative treatment methods, especially in brain surgery. Conventional MRI head coils can only partially meet the needs of intraoperative MR [6]. (c) Anxiety and claustrophobic reactions during brain MRI with a head coil. One study showed that the position or wearing of a head coil may impact anxiety levels [7]. Therefore, finding a method to replace the head coil for brain imaging will make MR applications more convenient.

The main motivation for the proposed study originates from the following. Digital surround technology (DST) combines the excellent signal-to-noise ratio (SNR) and sensitivity of high-density surface coils with superior uniformity of integrated radiofrequency bodies, resulting in richer and higher quality body imaging. This shows the potential to facilitate brain imaging with a DST body coil instead of using a head coil in conventional brain imaging. In addition, with continuous improvements in data availability and processing capacity in recent years, various deep learning (DL) applications in the field of medical imaging have naturally been developed. Many studies have shown that convolutional neural networks (CNNs) are more efficient than conventional methods for data processing and analysis, and related studies have also been conducted in the field of image enhancement [8-11].

*Research supported by the National Natural Science Foundation of China [Grant No. 61527807, 61931013], Beijing Scholar 2015 (Zhenchang Wang).

Y.-W. Liu and H.-J. Niu are with the School of Biological Science and Medical Engineering, Beihang University, Beijing, China; also with the Beijing Advanced Innovation Center for Biomedical Engineering, Beihang University, Beijing, China (e-mail: lyw_april@163.com; hjniu@buaa.edu.cn).

H.-X. Yin, P.-L. Ren, T.-T. Zhang, J. Li, H. Lv, and H.-Y. Ding are with the Department of Radiology, Beijing Friendship Hospital, Capital Medical University, Beijing, China (e-mail: 282496774@qq.com; yihan3469@126.com; tingting01981@hotmail.com; lijingxbhtr@163.com; chrislvhan@126.com; dingheyu1987@163.com). J.-J. Xia and J.-L. Ren are with GE Healthcare, China (e-mail: Jingjing-Xia@outlook.com; renjianliang@vip.qq.com).

Z.-C. Wang is with the School of Biological Science and Medical Engineering, Beihang University, Beijing, China; also with the Beijing Advanced Innovation Center for Biomedical Engineering, Beihang University, Beijing, China; also with the Department of Radiology, Beijing Friendship Hospital, Capital Medical University, Beijing, China. (corresponding author, phone: +86-13501163497; e-mail: cjr.wzhch@vip.163.com).

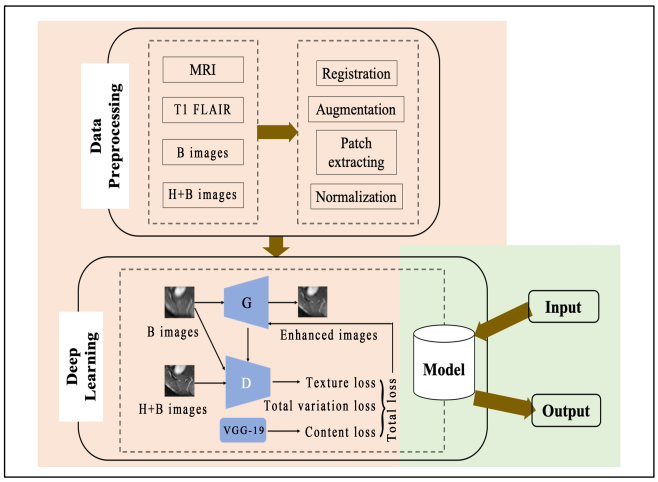


Figure 1. The workflow of the proposed deep-learning-based method. Two types of T1 FLAIR images composed the dataset. Data preprocessing was performed before training. The DL model was trained based on the SRGAN and VGG architectures. G = generator network, D = discriminator network.

In particular, a generative adversarial network (GAN) is a type of adversarial trained network that includes a generator network G and a discriminator network D [12].GANs have been applied to medical images for various purposes, such as noise reduction and resolution improvement [13-15].

We conducted this study to investigate the possibility of improving the quality of DST body coil imaging using a DL-based super resolution generative adversarial (SRGAN-VGG) network and to evaluate the potential of such methods to enable changes in the conventional scan mode of brain imaging.

## II. Materials and Methods

### A. Dataset

This study was approved by the Institutional Review Board of Beijing Friendship Hospital, Capital Medical University, and informed written consent was obtained. Forty healthy subjects were recruited in this study. None of the subjects had structural changes or signs of disease in the brain, and all subjects were older than 18 years. MRI scans were performed using a SIGNA Pioneer 3.0 T MRI scanner (GE Healthcare, Maukesha, WI, USA). Two types of T1 fluid-attenuated inversion recovery (FLAIR) images were obtained from each subject in this study: joint images of the head-neck coil and digital surround technology (DST) body coil (H+B images) and body coil images (B images). The head coil was removed from the scanner after the H+B image scan, and body coil brain imaging was performed. The imaging parameters were as follows: repetition time (TR), 1750 ms; echo time (TE), 21.1 ms; inversion time, 759.2 ms; matrix, 320×256; field of view (FOV), 22×22; slice thickness, 5 mm; and spacing between slices, 6 mm. Twenty-four image slices were obtained from each subject.

### B. Methodology

Fig. 1 shows the workflow of the proposed DL-based method. It includes two parts: data preprocessing and DL.

*1) Data preprocessing*

The H+B and B images were not perfectly aligned because the coils and the patient position were changed during the scan. Therefore, in the preprocessing steps, we performed image registration between H+B images and B images for the same subject to ensure that the two different types of images were coregistered to the same anatomical template as much as possible. Then, each image was cropped to nonoverlapping 100x100 patches for augmentation and random rotation of 90, 180, and 270 degrees for each patch. Furthermore, the min-max normalization method was used to normalize the various images.

*2) SRGAN-VGG*

The SRGAN-VGG architecture is based on the GAN and uses VGG to optimize the loss function. It consists of a generator network, G, a discriminator network, D, and the VGG network. The generator network for image enhancement begins with a 9x9 convolution filter followed by 4 residual blocks. Each residual block is composed of two 3x3 filters alternated with batch normalization layers. After the residual network, there are two additional 3x3 kernels and one 9x9 kernel. All convolutional kernels in the generator network consist of 64 channels and are followed by a rectified linear unit (ReLU) activation function, except for the last kernel, for which tanh activation is applied. In the discriminator network, 5 convolution filters, each followed by a leaky ReLU function, are used in our model. All kernels alternate with batch normalization layers except for the first layer. A sigmoid activation function is applied to the last fully connected layer to output the probability that the input image is a high-quality image. A pretrained VGG-19 network was used to extract the features.

*3) Loss function*

Texture loss, content loss and total variation loss were combined to form our final loss function in this study. The texture loss was defined as the cross-entropy loss function of the discriminator:

$$L_{texture}=-\sum_i \log D(G(I_p),I_g) \quad (1)$$

where G and D denote the generator and discriminator networks, respectively.

The VGG-19 network was implemented for feature map extraction, and the content loss was defined as the Euclidean distance between the feature maps of the enhanced and ground-truth images [12]:

$$L_{content}=\frac{1}{C_j H_j W_j}\sum_{x=1}^{W_j}\sum_{y=1}^{H_j}(\emptyset_j(G(I_p))_{x,y}-\emptyset_j(I_g)_{x,y})^2 \quad (2)$$

where Øj() denotes the feature map obtained from the j-th convolutional layer of the VGG-19 network, and $C_j$, $H_j$, and $W_j$ denote the channel number, height, and width, respectively, of this feature map.

The final total variation loss was designed to smooth the enhanced images:

$$L_{tv}=\frac{1}{CHW}\left\|\nabla_x G(I_p)+\nabla_y G(I_p)\right\| \quad (3)$$

where C, H, and W denote the channel number, height, and width, respectively, of the generated image.

The SRGAN-VGG network was trained on 36 subjects on a graphic processor (Quadro P4000, NVIDIA, Santa Clara, CA, USA) for 20k iterations with a batch size of 32 using the TensorFlow framework. The parameters of the network were optimized using the Adam optimizer via stochastic gradient descent with a learning rate of 5e-4. Images from the remaining 4 subjects were used for testing.

### *C. Evaluation methods and statistical analysis*

For full-reference image quality assessment, images in test data were segmented into gray matter (GM), white matter (WM) and cerebrospinal fluid (CSF) using SPM12 software (http://www.fil.ion.ucl.ac.uk/spm), and the model was quantitatively evaluated in terms of the mean square error (MSE), peak signal-to-noise ratio (PSNR), and structural similarity index (SSIM). No-reference image quality assessment methods — natural image quality evaluator (NIQE) and blind image quality index (BIQI) — were also used in this study. Notably, images with higher PSNR and SSIM values and lower MSE, BIQI, and NIQE values indicate better image quality. In addition, DL images and B images were qualitatively scored by two expert radiologists. The SNRs (SNR_Cortex, SNR_GM nuclei and SNR_WM nuclei), image contrast, image sharpness, and artifacts were evaluated according to the Likert five-point scale method and rated as follows: 1, very bad; 2, bad; 3, acceptable; 4, good; and 5, excellent [16].

Nonparametric Wilcoxon signed-rank tests were performed in R (version 3.5.1, http://www. r-project.org/) to compare the quantitative and qualitative assessment of the DL images and B images, respectively. The significance level was set to $P < .05$ (2-sided). The interrater reliability was assessed using the kappa coefficient based on the scores of each expert radiologist. The coefficient was interpreted as follows: almost perfect (0.81-1), substantial (0.61-0.80), moderate (0.41-0.60), fair (0.21-0.40), slight (0.01-0.20), or poor ($\leq 0$) reliability [17].

## III. Results and Discussion

The quantitative and qualitative assessments both showed that the image quality of the DL images was better than that of the B images. Fig. 2 shows a comparison of representative T1 FLAIR images consisting of B images, H+B images and DL images. Table I shows the f MSE, PSNR and SSIM values of B and DL images compared with H+B images in different tissues. All three image metrics were improved after DL. The SSIM value showed significant differences the GM, WM, and CSF. This implies that DL images have a higher structural similarity with high-quality images, which is very important for structure recognition and diagnosis in clinical practice. Table II shows that the NIQE and BIQI values of the DL images were significantly lower than those of the B images (all $P < .0001$). The results presented in Table I and Table II indicate that the DL images showed reduced image distortion and higher image quality.

Qualitative scoring results for the DL and B images are shown in Fig. 3. Compared with the B images, the DL images had higher scores for the SNRs (Cortex_SNR, SNR_GM nuclei and SNR_WM nuclei: $3.42 \pm 0.36$ versus $2.38 \pm 0.28$;

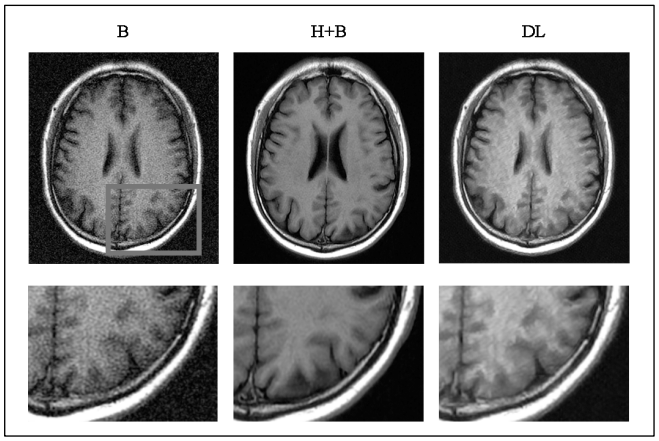


Figure 2. Representative results for a healthy subject. T1 FLAIR images are displayed for the DL results (top) and magnified views (bottom) of the body coil images (B), joint head-neck coil and body coil images (H+B) and deep learning images (DL).

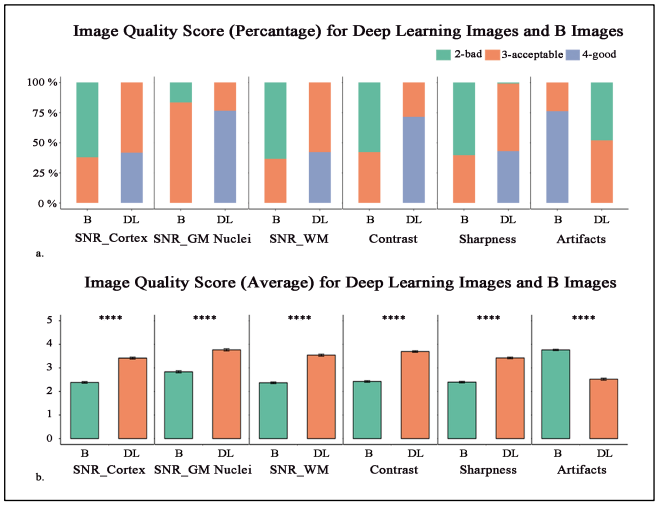


Figure 3. Comparison of the qualitative scoring results for the DL and B images. (a) Image quality scores as percentages for DL and B images when evaluated by blinded expert radiologists in terms of the SNR, image contrast, image sharpness, and artifacts. Each color bar represents the percentage of cases with a particular score. (b) Mean scores for DL and B images. Each color bar represents the mean score for a particular category. The error bars represent the standard error of the mean. DL = images reconstructed by deep learning, B = B images, WM = white matter, GM = gray matter, SNR = signal-to-noise ratio, **** = significant difference ($P < .0001$).

$3.77 \pm 0.25$ versus $2.83 \pm 0.24$; and $3.54 \pm 0.37$ versus $2.37 \pm 0.31$, respectively, all $P < .0001$), image contrast, and image sharpness ($3.69 \pm 0.29$ versus $2.42 \pm 0.31$, $3.42 \pm 0.29$ versus $2.40 \pm 0.29$, respectively, all $P < .0001$) and lower scores for artifacts ($2.52 \pm 0.37$ versus $3.76 \pm 0.25$, $P < .0001$). The kappa coefficients are mostly between 0.21 and 0.40, indicating fair agreement between the two observers. This may be due to the two radiologists having different amounts of experience and different understandings of DL images. These problems will be mitigated as the amount of data and the radiologists' experience increases and the methods are optimized.

A multiterm loss function including texture loss, content loss and total variation loss was used in this study. For medical images, content loss based on the pretrained VGG-19 network

TABLE I. MSE, PSNR AND SSIM VALUES OF B IMAGES AND DL IMAGES AGAINST H+B IMAGES IN DIFFERENT TISSUES

| Metrics | B Images | DL Images | P Value [a] |
|---|---|---|---|
| GM_MSE | 0.0428 ± 0.0138 | 0.0389 ± 0.0122 | < .05 |
| GM_PSNR | 14.0265 ± 1.9318 | 14.4145 ± 1.8435 | < .05 |
| GM_SSIM | 0.7977 ± 0.0568 | 0.8202 ± 0.0497 | < .0001 |
| WM_MSE | 0.0253 ± 0.0107 | 0.0231 ± 0.0094 | ns |
| WM_PSNR | 16.5625 ± 2.5865 | 16.8723 ± 2.3643 | ns |
| WM_SSIM | 0.8685 ± 0.0493 | 0.8868 ± 0.0407 | < .01 |
| CSF_MSE | 0.0248 ± 0.0069 | 0.0218 ± 0.0082 | < .01 |
| CSF_PSNR | 16.2080 ± 1.3663 | 16.4820 ± 1.4004 | < .05 |
| CSF_SSIM | 0.8560 ± 0.0320 | 0.8750 ± 0.0259 | < .0001 |

Data are presented as the means ± standard deviations. ns = no significance

a. Nonparametric Wilcoxon signed-rank test

TABLE II. NIQE AND BIQI VALUES FORB IMAGES AND DL IMAGES

| Metrics | B Images | DL Images | P Value [a] |
|---|---|---|---|
| NIQE | 5.7302 ± 0.4573 | 4.0018 ± 0.1688 | < .0001 |
| BIQI | 53.2126 ± 9.9170 | 29.6739 ± 1.8583 | < .0001 |

Data are presented as the means ± standard deviations. ns = no significance

a. Nonparametric Wilcoxon signed-rank test

encourages similar feature representations, including various aspects of image content and perceptual quality, rather than measuring the per-pixel differences between images. The total variation loss function was used to eliminate salt-and-pepper noise to some extent, resulting in smoother images. Therefore, the image SNR after DL is improved, resulting in better image contrast.

From a clinical perspective, the presented network will require further training to achieve sufficient performance for clinical applicability. However, the methodology is worthy of generalization. The following clinical prospects of the methodology are promising: (a) the proposed methodology may allow DST body coil imaging to be more widely used in clinical practice because of the potential to apply DL to obtain high-quality images from DST body coil data, and (b) the wider use of body coil imaging instead of head-neck coil imaging could enable more flexible subject examinations and reduce patient suffering during brain therapy.

## CONCLUSION

By applying a novel SRGAN-VGG-based DL method, we were able to enhance low-quality body coil brain images. The performance of the DL method was demonstrated on a small dataset, and the results suggest the possibility of applying DST body coils in brain imaging, thus making it feasible to modify the conventional scan mode of brain MRI and expand the use of MRI in clinical practice.

## ACKNOWLEDGMENT

The authors thank Zhoushe Zhao, PhD, for providing advice on data processing.

## REFERENCES

[1] E. Jensen and D. J. Crossman, "Technical review: Types of imaging-direct STORM," Anat. Rec., vol. 297, no. 12, pp. 2227–2231, 2014.

[2] S. Thorpe, P. M. Salkovskis, and A. Dittner, "Claustrophobia in MRI: the role of cognitions," Magn. Reson. Imaging, vol. 26, no. 8, pp. 1081–1088, 2008.

[3] L. Tellmann, H. H. Quick, A. Bockisch, H. Herzog, and T. Beyer, "The effect of MR surface coils on PET quantification in whole-body PET/MR: Results from a pseudo-PET/MR phantom study," Med. Phys., vol. 38, no. 5, pp. 2795–2805, 2011.

[4] C. Y.Sander, B. Keil, D. B.Chonde, B. R.Rosen, C. Catana, and L. L.Wald, "A 31-Channel MR Brain Array Coil Compatible with Positron Emission Tomography Christin," Physiol. Behav., vol. 176, no. 5, pp. 139–148, 2017.

[5] L. Isabel et al., "Design, Implementation, and Evaluation of a Head and Neck MRI RF Array Integrated with a 511 keV Transmission Source for Attenuation Correction in PET/MR," Sensors, vol. 19, 2019.

[6] K. Miki and K. Masamune, "High-resolution small field-of-view magnetic resonance image acquisition system using a small planar coil and a pneumatic manipulator in an open MRI scanner," Int. J. Comput. Assist. Radiol. Surg., vol. 10, no. 10, pp. 1687–1697, Oct. 2015.

[7] A. E. Napp et al., "Analysis and prediction of claustrophobia during MR imaging with the claustrophobia questionnaire: An observational prospective 18-month single-center study of 6500 patients," Radiology, vol. 283, no. 1, pp. 148–157, 2017.

[8] M. Mardani et al., "Deep generative adversarial neural networks for compressive sensing MRI," IEEE Trans. Med. Imaging, vol. 38, no. 1, pp. 167–179, 2019.

[9] K. H. Kim, S. H. Choi, and S. H. Park, "Improving arterial spin labeling by using deep learning," Radiology, vol. 287, no. 2, pp. 658–666, 2018.

[10] J. Shi, Q. Liu, C. Wang, Q. Zhang, S. Ying, and H. Xu, "Super-resolution reconstruction of MR image with a novel residual learning network algorithm," Phys. Med. Biol., vol. 63, no. 8, 2018.

[11] M. A. Mazurowski, M. Buda, A. Saha, and M. R. Bashir, "Deep learning in radiology: An overview of the concepts and a survey of the state of the art with focus on MRI," J. Magn. Reson. Imaging, vol. 49, no. 4, pp. 939–954, 2019.

[12] C. Ledig et al., "Photo-Realistic Single Image Super-Resolution Using a Generative Adversarial Network," Cvpr, vol. 2, no. 3, p. 4, 2017.

[13] M. Ran et al., "Denoising of 3D magnetic resonance images using a residual encoder–decoder Wasserstein generative adversarial network," Med. Image Anal., vol. 55, pp. 165–180, 2019.

[14] A. Hagiwara et al., "Improving the quality of synthetic FLAIR images with deep learning using a conditional generative adversarial network for pixel-by-pixel image translation," Am. J. Neuroradiol., vol. 40, no. 2, pp. 224–230, 2019.

[15] V. Ghodrati et al., "MR image reconstruction using deep learning: evaluation of network structure and loss functions," Quant. Imaging Med. Surg., vol. 9, no. 9, pp. 1516–1527, 2019.

[16] R. Likert, S. Roslow, and G. Murphy, "A Simple and Reliable Method of Scoring the Thurstone Attitude Scales," Pers. Psychol., vol. 46, no. 3, pp. 689–690, 2006.

[17] J. R. Landis and G. G. Koch, "The Measurement of Observer Agreement for Categorical Data," Biometrics, vol. 33, no. 1, pp. 159–174.